Achieving maximum scattering circular dichroism through the excitation of anapole states within chiral Mie nanospheres

Haifeng Hu [1,2,3] Qiaoqiang Gan,[4,*] and Qiwen Zhan [1,2,3,†]

[1]*School of Optical-Electrical and Computer Engineering, University of Shanghai for Science and Technology, Shanghai 200093, China*

[2]*Zhangjiang Laboratory, 100 Haike Road, Shanghai 201204, China*

[3]*Shanghai Key Lab of Modern Optical System, University of Shanghai for Science and Technology, Shanghai 200093, China*

[4]*Material Science Engineering, King Abdullah University of Science and Technology, Thuwal 23955-6900, Kingdom of Saudi Arabia*

(Received 16 January 2022; revised 3 May 2022; accepted 7 June 2022; published 17 June 2022)

The chirality-dependent asymmetric light-matter interaction can be enhanced using various artificial photonic structures as well as engineered incident field. Compared with chiral photonic structures, the engineered optical field is less explored and recently recognized as a new regime in tailoring light-matter interaction. In this work, we demonstrate that weakly chiral spheres can exhibit the maximum scattering circular dichroism (CD) by tailoring the incident field to construct chirality-sensitive anapole states. By considering the chiral terms radiated from Mie nanospheres as perturbation, a multiscattering model is established to predict the chiroptical Mie scattering response of these nanospheres. This model provides a specific guideline to tailor the incident field to realize the upper limit of the achievable scattering CD.

DOI: 10.1103/PhysRevB.105.245412

I. INTRODUCTION

Chirality describes the structural properties of three-dimensional objects that cannot be superimposed onto their mirror images [1]. It has been proved that an infinite number of pseudoscalars can be constructed to quantify the chirality of a geometric object [2]. With just one nonzero pseudoscalar, the object is chiral. Therefore, no golden standard is available to quantitatively evaluate or compare the degree of geometric chirality. Instead of geometry, an alternative way to evaluate chirality of an object is based on its light-matter interaction. For example, a chiral object may respond differently to circularly polarized light (CPL) with opposite handedness, resulting in chiroptical effects such as circular dichroism (CD) [1]. Conventionally, the CD signal is defined as $g = 2(W^+ - W^-)/(W^+ + W^-)$, where $W^{\pm}$ is the absorption (or scattering) power under left/right-handed CPL. This technique has been widely used to characterize the chirality of chemical and biomolecules whose CD signals are mostly very weak (e.g., [3]). In recent years, extensive effort has been devoted to design and fabricate nanostructures with enhanced CD responses [4–8] (e.g., using plasmonic helices [9], nanocavities [10], and metasurfaces [11]). The theoretical upper limit of CD is $g = 2$ (e.g., when W^- is zero but W^+ is nonzero), indicating that the object can interact with one handedness of CPL beam, but not with the opposite handedness [12]. For instance, a complex metasurface was designed theoretically to obtain the maximum CD enabled by bound states in the continuum [13]. This maximum CD effect can be interpreted as the perfect match between the geometrical chirality of the designed structures and the CPL field.

On the other hand, a more general definition of CD has been proposed to describe the chiral response of objects under arbitrary light fields rather than the two orthogonal CPL states [14]. Using this general parameter, the maximum CD can also be realized by using light field engineered to match the chiral features of a given object instead of designing structural objects. Optical chirality (also called Lipkin's 00-zilch [15]) is defined as $C = (\varepsilon_0 \mathbf{E} \cdot \nabla \times \mathbf{E} + \mu_0 \mathbf{H} \cdot \nabla \times \mathbf{H})/2$, describing the local chiral feature of a light field [14]. For a point chiral dipole, the intensity of the CD signal is proved to be proportional to the local C value. Thus, in the past decade a significant amount effort has been devoted to realize superchiral light with larger C values than CPL beams to enhance CD signals [14,16–20]. In Ref. [7], the chiral response of nanostructures can be enhanced by optimizing the incident field in the far field region. However, the optical chirality C cannot represent the global chiral features of the entire light field. If the size of the object is beyond the Rayleigh regime (i.e., large objects that are not much smaller than the wavelength), the contributions of high order multipole moments to the chiral response cannot be neglected [14,21]. As a result, the C value is inappropriate to predict the chiral interaction between these large Mie particles and the light field. Recently, experimental works have demonstrated that scattering CD by a large chiral structure can be enhanced to $g = 1.2$ by increasing the topological charge of the incident light [22]. Therefore, the global feature of the light field (e.g., topological charge) is closely related to the chiral response of Mie particles. One of the key fundamental questions is how to design the light field globally to enhance and even maximize the CD signal for a chiral Mie particle.

In this work, we develop a multiscattering model that can be used to calculate the value of the scattering CD signal quantitatively. Using this model, the specific conditions of the global optical field can be determined to realize the maximum

*Corresponding author: qiaoqiang.gan@kaust.edu.sa

†Corresponding author: qwzhan@usst.edu.cn

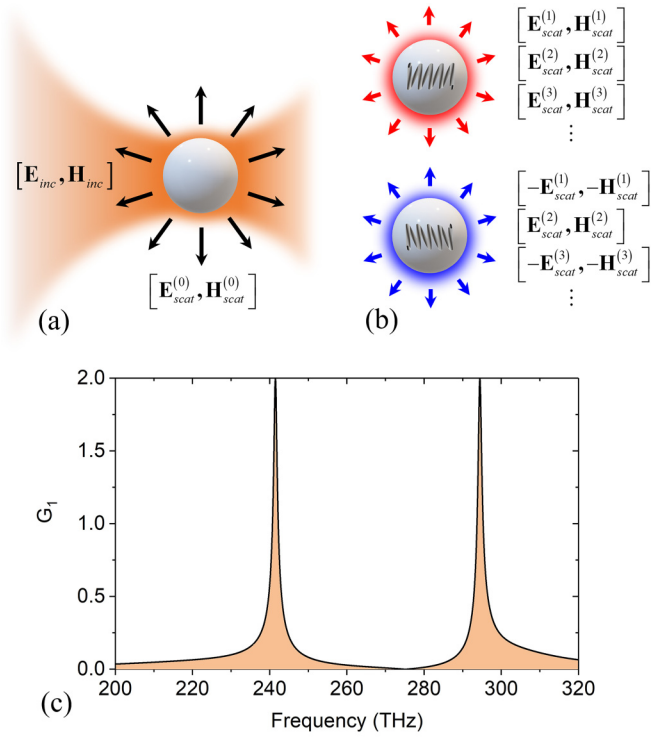

FIG. 1. The theoretical model is demonstrated in (a) and (b). (a) The zeroth-order scattering process by the reference system (i.e., the nonchiral sphere). (b) The high order scattering fields radiated by the localized sources in two spheres with the opposite chirality. (c) The upper limit of scattering CD by sphere with weak chirality when the incident field consists of VSHs with the order of (1, 1).

CD signal for a Mie sphere made of chiral materials. Under the designed optimized optical fields, the upper limit of CD value (i.e., $g = 2$) can be realized at specific frequencies due to the excitation of anapole states.

II. MULTISCATTERING MODEL FOR CHIRAL SPHERE

To predict the scattering CD from Mie spheres, here we propose a multiscattering model based on the Lorentz-Mie theory [23]. When the chirality of a sphere is weak, the influence of its chiral property can be considered as a perturbation in the model [8]. The basic route of this method contains two steps: Step 1 is to analyze the reference structure by removing the chirality of the sphere [Fig. 1(a)]. The zeroth-order scattering field $[\mathbf{E}^{(0)}_{\text{scat}}, \mathbf{H}^{(0)}_{\text{scat}}]$ and the field inside the sphere, $[\mathbf{E}^{(0)}_1, \mathbf{H}^{(0)}_1]$, are both calculated by the Lorentz-Mie theory [23]. Step 2 is to consider the interaction between the zeroth-order scattering field and the chiral features to solve the secondary scattering field [Fig. 1(b)]. The first-order perturbing sources of current and magnetization can produce the outgoing waves from the internal sphere region. The transmitted and reflected fields through the sphere surface are denoted as $[\mathbf{E}^{(1)}_{\text{scat}}, \mathbf{H}^{(1)}_{\text{scat}}]$ and $[\mathbf{E}^{(1)}_1, \mathbf{H}^{(1)}_1]$, respectively. The first order inner field of $[\mathbf{E}^{(1)}_1, \mathbf{H}^{(1)}_1]$ can further excite other perturbing sources and high order scattering fields of $[\mathbf{E}^{(l)}_{\text{scat}}, \mathbf{H}^{(l)}_{\text{scat}}]$ with $l > 1$. The total scattering fields are contributed by the direct scattering fields from the nonchiral sphere and the secondary scattering fields from nonzero order perturbing sources. In Fig. 1(b), the secondary scattering fields by two spheres with opposite chiralities (i.e., enantiomers) are compared. By switching the chirality of the sphere, the sign of scattering field is changed for odd-order terms, while unchanged for even-order terms. Using this multiscattering model, the total scattering field can be decomposed into the chiral part and nonchiral part rigorously. Next, the details of this model are discussed.

The constitutive relations of the reciprocal and chiral media inside a homogeneous sphere can be expressed as [24]

$$\mathbf{D} = \varepsilon_s \mathbf{E} - i\kappa_s \mathbf{H}, \tag{1}$$

$$\mathbf{B} = \mu_s \mathbf{H} + i\kappa_s \mathbf{E}. \tag{2}$$

Here ε_s and μ_s are the permittivity and permeability of sphere; κ_s is the chiral parameter. The scattering field by removing the chiral feature of the sphere (i.e., $\kappa_s = 0$) is considered first. In the frame of Lorentz-Mie theory [23], the scattering field by a Mie sphere should be expanded as the linear combination of the vector spherical harmonics (VSHs) as

$$\mathbf{E}^{(0)}_{\text{scat}} = \sum_{n=1}^{+\infty} \sum_{m=-n}^{n} \left[a^{(0)}_{mn} \mathbf{M}_{mn}(k_0, \mathbf{r}) + b^{(0)}_{mn} \mathbf{N}_{mn}(k_0, \mathbf{r}) \right], \tag{3}$$

$$\mathbf{H}^{(0)}_{\text{scat}} = \frac{1}{iZ_0} \sum_{n=1}^{+\infty} \sum_{m=-n}^{n} \left[a^{(0)}_{mn} \mathbf{N}_{mn}(k_0, \mathbf{r}) + b^{(0)}_{mn} \mathbf{M}_{mn}(k_0, \mathbf{r}) \right]. \tag{4}$$

In Eqs. (3) and (4), k_0 and Z_0 are the vacuum wave vector and vacuum impedance. $a^{(0)}_{mn}$ and $b^{(0)}_{mn}$ are the scattering coefficients. The expressions with the superscript of "(0)" are associated with the reference structure, i.e., the nonchiral sphere in free space. The incident field and the internal field of the sphere can also be expressed as the combination of VSHs, i.e.,

$$\mathbf{E}_{\text{inc}} = \sum_{n=1}^{+\infty} \sum_{m=-n}^{n} \left[u^{(0)}_{mn} Rg\mathbf{M}_{mn}(k_0, \mathbf{r}) + v^{(0)}_{mn} Rg\mathbf{N}_{mn}(k_0, \mathbf{r}) \right], \tag{5}$$

$$\mathbf{H}_{\text{inc}} = \frac{1}{iZ_0} \sum_{n=1}^{+\infty} \sum_{m=-n}^{n} \left[u^{(0)}_{mn} Rg\mathbf{N}_{mn}(k_0, \mathbf{r}) + v^{(0)}_{mn} Rg\mathbf{M}_{mn}(k_0, \mathbf{r}) \right], \tag{6}$$

$$\mathbf{E}^{(0)}_1 = \sum_{n=1}^{+\infty} \sum_{m=-n}^{n} \left[c^{(0)}_{mn} Rg\mathbf{M}_{mn}(k_1, \mathbf{r}) + d^{(0)}_{mn} Rg\mathbf{N}_{mn}(k_1, \mathbf{r}) \right], \tag{7}$$

$$\mathbf{H}^{(0)}_1 = \frac{1}{iZ_1} \sum_{n=1}^{+\infty} \sum_{m=-n}^{n} \left[c^{(0)}_{mn} Rg\mathbf{N}_{mn}(k_1, \mathbf{r}) + d^{(0)}_{mn} Rg\mathbf{M}_{mn}(k_1, \mathbf{r}) \right]. \tag{8}$$

To avoid the singularity at the origin (i.e., the center of the sphere), the incident field and internal field are expressed as the combination of regular VSHs (i.e., $Rg\mathbf{M}_{mn}$, $Rg\mathbf{N}_{mn}$). In Eqs. (7) and (8), $k_1 = (\varepsilon_s \mu_s)^{1/2} k_0$ and $Z_1 = (\mu_s/\varepsilon_s)^{1/2}$. By

applying the boundary conditions at the surface of the sphere, the unknown expansion coefficients in scattering field and the internal field can be calculated by $u_{mn}^{(0)}$ and $v_{mn}^{(0)}$,

$$a_{mn}^{(0)} = T_n^a u_{mn}^{(0)}, \tag{9}$$

$$b_{mn}^{(0)} = T_n^b v_{mn}^{(0)}, \tag{10}$$

$$c_{mn}^{(0)} = T_n^c u_{mn}^{(0)}, \tag{11}$$

$$d_{mn}^{(0)} = T_n^d v_{mn}^{(0)}. \tag{12}$$

In Eqs. (9)–(12), the coefficients of T_n^a, T_n^b, T_n^c and T_n^d are given in Appendix A. When the chiral property is introduced into the sphere, the scattering field will deviate from the nonchiral case (i.e., in the reference structure). In our model, the terms including κ_s in Eqs. (1) and (2) are considered as the perturbing sources that produce the localized distributions of current $\mathbf{J}^{(1)}$ and magnetization $\mathbf{M}^{(1)}$ inside the sphere. These perturbing sources are expressed as $\mathbf{J}^{(1)} = -\omega\kappa_s\mathbf{H}_1$ and $\mathbf{M}^{(1)} = i(\kappa_s/\mu)\mathbf{E}_1$. It should be noted that $[\mathbf{E}_1, \mathbf{H}_1]$ are calculated in the sphere with chirality. For materials with weak chirality (i.e., a usual case for existing natural materials), the internal field of $[\mathbf{E}_1, \mathbf{H}_1]$ can be approximately replaced by $[\mathbf{E}_1^{(0)}, \mathbf{H}_1^{(0)}]$ in Eqs. (7) and (8). The radiation field of $[\mathbf{E}_{\text{inc}}^{(1)}, \mathbf{H}_{\text{inc}}^{(1)}]$ by $\mathbf{J}^{(1)}$ and $\mathbf{M}^{(1)}$ can be obtained by solving the following inhomogeneous wave equations:

$$\left(\nabla^2 + k_1^2\right)\left[\mathbf{r}\cdot\mathbf{E}_{\text{inc}}^{(1)}\right] = k_1 Z_1 \hat{\mathbf{L}}\cdot\left[\mathbf{M}^{(1)} + \frac{1}{k_1^2}\nabla\times\mathbf{J}^{(1)}\right], \tag{13}$$

$$\left(\nabla^2 + k_1^2\right)\left[\mathbf{r}\cdot\mathbf{H}_{\text{inc}}^{(1)}\right] = -i\hat{\mathbf{L}}\cdot[\mathbf{J}^{(1)} + \nabla\times\mathbf{M}^{(1)}]. \tag{14}$$

In Eqs. (13) and (14), the angular momentum operator is defined as $\hat{\mathbf{L}} = -i\mathbf{r}\times\nabla$. The Green's function for the wave equations is $G_1(\mathbf{r}, \mathbf{r}') = e^{ik_1|\mathbf{r}-\mathbf{r}'|}/|\mathbf{r}-\mathbf{r}'|$, which can be expended by spherical harmonics as [25]

$$G(\mathbf{r}, \mathbf{r}') = ik_1 \sum_{n=0}^{+\infty} j_n(k_1 r') h_n^{(1)}(k_1 r) \sum_{m=-n}^{n} (-1)^m (2n+1) Y_n^{-m}(\theta', \phi') Y_n^m(\theta, \phi), \tag{15}$$

which is only applicable for $r > r'$. In this work, the scalar spherical harmonics are defined as $Y_n^m = P_n^m(\cos\theta)e^{im\phi}$ At the inner surface of the sphere (i.e. $|\mathbf{r}| = R_s^-$), the secondary incident field radiated by $\mathbf{J}^{(1)}$ and $\mathbf{M}^{(1)}$ is expressed as the sum of outgoing VSHs:

$$\mathbf{E}_{\text{inc}}^{(1)} = \sum_{n=1}^{+\infty}\sum_{m=-n}^{n}\left[u_{mn}^{(1)}\mathbf{M}_{mn}(k_1, \mathbf{r}) + v_{mn}^{(1)}\mathbf{N}_{mn}(k_1, \mathbf{r})\right], \tag{16}$$

$$\mathbf{H}_{\text{inc}}^{(1)} = \frac{1}{iZ_1}\sum_{n=1}^{+\infty}\sum_{m=-n}^{n}\left[u_{mn}^{(1)}\mathbf{N}_{mn}(k_1, \mathbf{r}) + v_{mn}^{(1)}\mathbf{M}_{mn}(k_1, \mathbf{r})\right]. \tag{17}$$

Following the derivation in the textbook [25], the expansion coefficients can be calculated by the integrals over the secondary radiation sources:

$$u_{mn}^{(1)} = \frac{k_1^2 Z_1}{\gamma_{mn}}\int_V Y_n^{-m}(\theta,\phi)\begin{Bmatrix} j_n(k_1 r)[\nabla\cdot(\mathbf{r}\times\mathbf{J}^{(1)})] + \frac{\partial}{\partial r}[r j_n(k_1 r)](\nabla\cdot\mathbf{M}^{(1)}) \\ -k_1^2 j_n(k_1 r)[(\mathbf{r}\cdot\mathbf{M}^{(1)})] \end{Bmatrix} d^3\mathbf{r}, \tag{18}$$

$$v_{mn}^{(1)} = \frac{ik_1^2 Z_1}{\gamma_{mn}}\int_V Y_n^{-m}(\theta,\phi)\begin{Bmatrix} \frac{1}{\sqrt{\varepsilon_1\mu_1}}\rho(\mathbf{r})\frac{\partial}{\partial r}[r j_n(k_1 r)] + ik_1 j_n(k_1 r)(\mathbf{r}\cdot\mathbf{J}^{(1)}) \\ -ik_1 j_n(k_1 r)\nabla\cdot(\mathbf{r}\times\mathbf{M}^{(1)}) \end{Bmatrix} d^3\mathbf{r}. \tag{19}$$

After some mathematical derivations, Eqs. (18) and (19) can be simplified as

$$u_{mn}^{(1)} = \kappa_1 F_n(k_1 R_s) d_{mn}^{(0)}, \tag{20}$$

$$v_{mn}^{(1)} = \kappa_1 F_n(k_1 R_s) c_{mn}^{(0)}. \tag{21}$$

The definition of $F_n(x)$ is $F_n(x) = -i(\varepsilon_1\mu_1)^{-1/2}[\psi'_n(x)\psi_n(x) + 2\int_0^x \psi_n^2(\alpha)d\alpha]$. The secondary incident field radiates from the internal sphere region. The scattering process by sphere surface should be considered in our model. The transmission and reflection field are defined as scattering field and internal field excited by the first-order perturbing sources. These fields are indicated by the superscript "(1)." These first-order perturbing fields can also be expanded by VSHs as

$$\mathbf{E}_{\text{scat}}^{(1)} = \sum_{n=1}^{+\infty}\sum_{m=-n}^{n}\left[a_{mn}^{(1)}\mathbf{M}_{mn}(k_0, \mathbf{r}) + b_{mn}^{(1)}\mathbf{N}_{mn}(k_0, \mathbf{r})\right], \tag{22}$$

$$\mathbf{H}_{\text{scat}}^{(1)} = \frac{1}{iZ_0}\sum_{n=1}^{+\infty}\sum_{m=-n}^{n}\left[a_{mn}^{(1)}\mathbf{N}_{mn}(k_0, \mathbf{r}) + b_{mn}^{(1)}\mathbf{M}_{mn}(k_0, \mathbf{r})\right], \tag{23}$$

$$\mathbf{E}_1^{(1)} = \sum_{n=1}^{+\infty}\sum_{m=-n}^{n}\left[c_{mn}^{(1)}Rg\mathbf{M}_{mn}(k_1,\mathbf{r}) + d_{mn}^{(1)}Rg\mathbf{N}_{mn}(k_1,\mathbf{r})\right], \tag{24}$$

$$\mathbf{H}_1^{(1)} = \frac{1}{iZ_1}\sum_{n=1}^{+\infty}\sum_{m=-n}^{n}\left[c_{mn}^{(1)}Rg\mathbf{N}_{mn}(k_1,\mathbf{r}) + d_{mn}^{(1)}Rg\mathbf{M}_{mn}(k_1,\mathbf{r})\right]. \tag{25}$$

The expansion coefficients can be calculated to be

$$a_{mn}^{(1)} = S_n^a u_{mn}^{(1)}, \tag{26}$$

$$b_{mn}^{(1)} = S_n^b v_{mn}^{(1)}, \tag{27}$$

$$c_{mn}^{(1)} = S_n^c u_{mn}^{(1)}, \tag{28}$$

$$d_{mn}^{(1)} = S_n^d v_{mn}^{(1)}. \tag{29}$$

In Eqs. (26–29), the coefficients of S_n^a, S_n^b, S_n^c, and S_n^d are given in Appendix A. As shown in Fig. 1(b), when the chirality of the sphere is inversed (i.e., $\kappa_s \to -\kappa_s$), the sign of scattering field $[\mathbf{E}_{\text{scat}}^{(1)}, \mathbf{H}_{\text{scat}}^{(1)}]$ will be changed. The scattering circular dichroism is introduced by the secondary scattering field. Meanwhile, the internal field $[\mathbf{E}_1^{(1)}, \mathbf{H}_1^{(1)}]$ can produce second order current $\mathbf{J}^{(2)}$ and magnetization $\mathbf{M}^{(2)}$, whose magnitude is related to κ_1^2. Therefore, the scattering field $[\mathbf{E}_{\text{scat}}^{(2)}, \mathbf{H}_{\text{scat}}^{(2)}]$ produced by $\mathbf{J}^{(2)}$ and $\mathbf{M}^{(2)}$ are nonchiral. Following this procedure, the high order sources can be also calculated. The total scattering field can be expressed as the sum of all the terms associated with different orders of perturbing sources. The total scattering coefficients a_{mn} and b_{mn} can be divided into nonchiral and chiral parts, respectively, i.e.,

$$a_{mn}(\pm\kappa_1) = A_{mn} \pm A'_{mn}, \tag{30}$$

$$b_{mn}(\pm\kappa_1) = B_{mn} \pm B'_{mn}, \tag{31}$$

where m and n are integers to denote the orders of VSH field. Here A_{mn} and B_{mn} are nonchiral parts, while A'_{mn} and B'_{mn} are chiral parts. The nonchiral parts of a_{mn} and b_{mn} are composed by the even-order coefficients, which are unchanged during the chirality inversion, while the chiral parts are contributed by the odd-order coefficients. Here,

$$A_{mn} = \Gamma_n^{(a)} u_{mn}, \tag{32}$$

$$A'_{mn} = \gamma_n^{(a)} v_{mn}, \tag{33}$$

$$B_{mn} = \Gamma_n^{(b)} v_{mn}, \tag{34}$$

$$B'_{mn} = \gamma_n^{(b)} u_{mn}. \tag{35}$$

In Eqs. (32)–(35), the coefficients of $\Gamma_n^{(a)}$, $\gamma_n^{(a)}$, $\Gamma_n^{(b)}$, and $\gamma_n^{(b)}$ can be expressed as

$$\Gamma_n^{(a)} = \left[T_n^a + \frac{\kappa_1^2 F^2 S_n^a S_n^d T_n^c}{1-\kappa_1^2 F_n^2 S_n^c S_n^d}\right], \tag{36}$$

$$\gamma_n^{(a)} = \frac{\kappa_1 F_n S_n^a T_n^d}{1-\kappa_1^2 F_n^2 S_n^c S_n^d}, \tag{37}$$

$$\Gamma_n^{(b)} = \left[T_n^b + \frac{\kappa_1^2 F_n^2 S_n^b S_n^c T_n^d}{1-\kappa_1^2 F_n^2 S_n^c S_n^d}\right], \tag{38}$$

$$\gamma_n^{(b)} = \frac{\kappa_1 F_n S_n^b T_n^c}{1-\kappa_1^2 F_n^2 S_n^c S_n^d}. \tag{39}$$

The total scattering power by the chiral sphere can be calculated by the scattering coefficients of a_{mn} and b_{mn} in Eq. (40) [23],

$$W = \frac{1}{2k_0^2}\sum_{n=1}^{+\infty}\sum_{m=-n}^{n}\left[|a_{mn}|^2 + |b_{mn}|^2\right]. \tag{40}$$

As discussed in the Introduction, the generalized CD of a chiral sphere can be determined by values of W^+ and W^-, which are the scattering power under the illuminations of arbitrary field and the corresponding mirror field. By taking the mirror operation on the chiral sphere and optical field simultaneously, the scattering power remains the same. Therefore, W^+ and W^- equal the scattering powers of the chiral sphere with κ_s and the mirror sphere with $-\kappa_s$ under the same incident field in Eq. (41),

$$W^{\pm} = \frac{1}{2k_0^2}\sum_{n=1}^{+\infty}\sum_{m=-n}^{n}\left[|A_{mn} \pm A'_{mn}|^2 + |B_{mn} \pm B'_{mn}|^2\right]. \tag{41}$$

Therefore, based on Eqs. (32)–(35) in the multiscattering model, the value of the scattering CD can be directly calculated by the expansion coefficients of u_{mn} and v_{mn}.

III. PREDICTION OF MAXIMUM SCATTERING CD

Next, we implement this model to predict the maximum CD scattering condition for a homogeneous chiral sphere. When the incident field is a linear combination of two regular VSHs with the same order, i.e., $u_{mn}Rg\mathbf{M}_{mn} + v_{mn}Rg\mathbf{N}_{mn}$, the scattering CD can then be expressed as

$$g_{mn} = \frac{4\text{Re}\left[\left(\Gamma_n^{(a)}\gamma_n^{(a)*} + \Gamma_n^{(b)*}\gamma_n^{(b)}\right)u_{mn}v_{mn}^*\right]}{\left(\left|\Gamma_n^{(a)}\right|^2 + \left|\gamma_n^{(b)}\right|^2\right)|u_{mn}|^2 + \left(\left|\Gamma_n^{(b)}\right|^2 + \left|\gamma_n^{(a)}\right|^2\right)|v_{mn}|^2}. \tag{42}$$

Using Eq. (42), one can obtain the upper limit of the CD value related to the order of (m, n). It can be proved that the upper limit of $|g_{mn}|$ should be G_n, which can be expressed as

$$G_n = \frac{2\left|\Gamma_n^{(a)}\gamma_n^{(a)*} + \Gamma_n^{(b)*}\gamma_n^{(b)}\right|}{\sqrt{\left|\Gamma_n^{(a)}\right|^2 + \left|\gamma_n^{(b)}\right|^2}\sqrt{\left|\Gamma_n^{(b)}\right|^2 + \left|\gamma_n^{(a)}\right|^2}}. \tag{43}$$

The condition to obtain the maximum value of $g_{mn} = G_n$ is

$$\frac{u_{mn}}{v_{mn}} = e^{-i\Psi}\sqrt{\left|\gamma_n^{(a)}\right|^2 + \left|\Gamma_n^{(b)}\right|^2}\Big/\sqrt{\left|\gamma_n^{(b)}\right|^2 + \left|\Gamma_n^{(a)}\right|^2}, \tag{44}$$

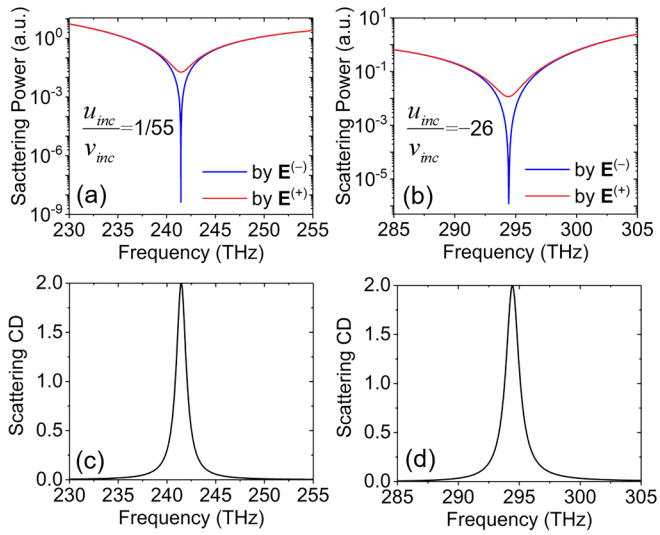

FIG. 2. The spectra of scattering power and CD for the chiral sphere under tailored fields of $\mathbf{E}^{(\pm)}$. (a) Scattering power spectra when $u_{\rm inc}/v_{\rm inc} = 1/55$. (b) Scattering power spectra when $u_{\rm inc}/v_{\rm inc} = -26$. The blue and red lines in (a) and (b) represents the results under $\mathbf{E}^{(-)}$ and $\mathbf{E}^{(+)}$. (c) The scattering CD spectrum when $u_{\rm inc}/v_{\rm inc} = 1/55$. (d) The scattering CD spectrum when $u_{\rm inc}/v_{\rm inc} = -26$.

where Ψ is the complex phase of $\Gamma_n^{(a)}\gamma_n^{(a)*} + \Gamma_n^{(b)*}\gamma_n^{(b)}$. Using Eq. (43), the upper limit of scattering CD, G_1, for the order of $n = 1$, is plotted in Fig. 1(c). In this calculation, the radius of the sphere is 320 nm, $\varepsilon_1 = 9$, $\mu_1 = 1$, and $\kappa_1 = 0.01$. Intriguingly, one can see two peaks at the frequencies of 241.46 and 294.46 THz, where the CD values can reach the maximum value of $g = 2$. Importantly, using Eq. (44), one can determine the incident field for the Mie sphere to realize these maximum CD scattering values, as will be explained next.

To determine the required optical field to realize the maximum scattering CD, here we calculate the scattering CD spectra. The incident field consists of two VSHs with $(m, n) = (1, 1)$, i.e., $\mathbf{E}^{(+)} = u_{\rm inc}Rg\mathbf{M}_{1,1} + v_{\rm inc}Rg\mathbf{N}_{1,1}$. According to Eq. (44), the peak condition for $G_1 = 2$ in Fig. 1(c) were realized when $u_{\rm inc}/v_{\rm inc} = 1/55$ and $u_{\rm inc}/v_{\rm inc} = -26$. The scattering spectra of the chiral sphere under $\mathbf{E}^{(+)}$ are shown by the red curves in Figs. 2(a) and 2(b), respectively. To obtain the CD value, the scattering spectra should be calculated under the incident field after mirror operation, i.e., $\mathbf{E}^{(-)} = u_{\rm inc}Rg\mathbf{M}_{-1,1} - v_{\rm inc}Rg\mathbf{N}_{-1,1}$ (see Appendix B). Under the illumination of $\mathbf{E}^{(-)}$, the scattering spectra of the chiral sphere are shown by the blue curves in Figs. 2(a) and 2(b). In these cases, the scattering power drops to zero at the frequencies of 241.46 and 294.46 THz, indicating the completely suppressed scattering field from the sphere. The corresponding scattering CD spectra for these two pairs of incident fields are calculated using $g = 2(W^+ - W^-)/(W^+ + W^-)$ as shown in Figs. 2(c) and 2(d). One can see that the maximum scattering CD signal is achieved in the sphere enabled by the complete nonscattering states. In contrast, under the illumination of CPL, the value of scattering CD from the same sphere is −0.114–0.054 in the frequency range [176.5, 333.3 THz] (see Appendix C).

It should be noted that although the upper limit of scattering CD in Eq. (43) is only applicable for the incident field of $u_{mn}Rg\mathbf{M}_{mn} + v_{mn}Rg\mathbf{N}_{mn}$ with a given order of (m, n), it can be generalized to cases with arbitrary incident fields of $\sum_{n=1}^{N}\sum_{m=-n}^{n} u_{mn}Rg\mathbf{M}_{mn} + v_{mn}Rg\mathbf{N}_{mn}$. For simplicity, the incident field is only consisting of two orders of VSHs. Therefore, the scattering powers under two incident fields (i.e., mirror images of each other) can be expressed as

$$W^+ = W_1^+ + W_2^+, \tag{45}$$

$$W^- = W_1^- + W_2^-. \tag{46}$$

The following two parameters are defined as

$$g_1 = 2(W_1^+ - W_1^-)/(W_1^+ + W_1^-), \tag{47}$$

$$g_2 = 2(W_2^+ - W_2^-)/(W_2^+ + W_2^-). \tag{48}$$

Because the scattering power is positive, $g_1 \in [-2, 2]$ and $g_2 \in [-2, 2]$. The scattering CD can be expressed as

$$g = \frac{g_1(W_1^+ + W_1^-) + g_2(W_2^+ + W_2^-)}{W_1^+ + W_1^- + W_2^+ + W_2^-}. \tag{49}$$

Without loss of generality, we assume that $g_1 > g_2$, then

$$g = g_1 + \frac{(W_2^+ + W_2^-)(g_2 - g_1)}{W_1^+ + W_1^- + W_2^+ + W_2^-} \leqslant g_1, \tag{50}$$

$$g = g_2 + \frac{(W_1^+ + W_1^-)(g_1 - g_2)}{W_1^+ + W_1^- + W_2^+ + W_2^-} \geqslant g_2. \tag{51}$$

Therefore, it can be proved that $\min(g_1, g_2) \leqslant g \leqslant \max(g_1, g_2)$. This conclusion can easily be generalized to the case with more orders of VSHs, i.e., $\min(g_1, g_2, \ldots) \leqslant g \leqslant \max(g_1, g_2, \ldots)$. Therefore, the absolute value of g_{mn} is limited by G_n, so that $\min(-G_1, -G_2, \ldots) \leqslant g \leqslant \max(G_1, G_2, \ldots)$.

IV. CHIRALITY-SENSITIVE ANAPOLE

To reveal the physics of the maximum CD under the designed optical field, we then employ the multipole expansion method to model the chiral scattering [21,25]. The scattering field is radiated by the oscillation current $\mathbf{J}$ and magnetization $\mathbf{M}$ which are excited by the field inside the sphere. The scattering fields are mainly radiated by the magnetic dipole (MD, induced by $\mathbf{J}$), electric dipole (ED), and toroidal dipole (TD). For the maximum scattering CD condition with $u_{\rm inc}/v_{\rm inc} = -26$, amplitudes of the three moments for the sphere as well as the electric and magnetic scattering coefficients (i.e., a_1 and b_1) under the incident field of $\mathbf{E}^{(-)}$ are calculated in Fig. 3. At the frequency of 294.463 THz, both scattering coefficients a_1 [Fig. 3(a)] and b_1 [Fig. 3(b)] are zero, indicating that the sphere is at the completely nonradiating state. Specifically, a_1 can be well predicted by the amplitude of MD [Fig. 3(a)], while b_1 is mainly contributed by ED and TD [see the amplitudes of b_1, ED, and TD in Fig. 3(b), and phases of ED and TD in Fig. 3(c)]. Specifically, at $f = 294.46$ THz, the amplitudes of ED and TD are equal, but their phases are the opposite [see the vertical dashed line in Fig. 3(c)]. As a result, identical radiation patterns of ED and TD in the far field can

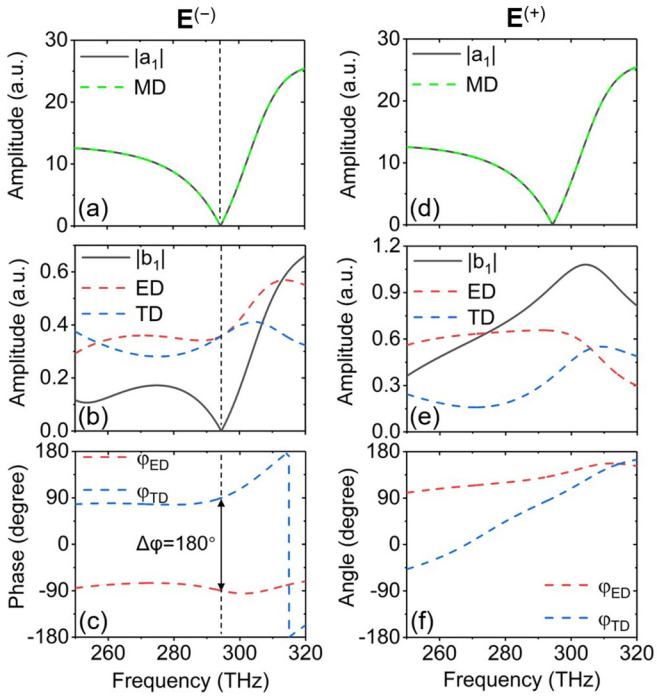

FIG. 3. The spectra of scattering coefficients and the complex amplitudes of three types dipoles. The results in (a)–(c) are under the incidence of $\mathbf{E}^{(-)}$ and in (d)–(f) for $\mathbf{E}^{(+)}$. The green dashed curves represent the amplitude of MD in (a) and (d). The blue and red dashed curves represent the amplitudes of ED and TD in (b) and (e), and their phases in (c) and (f), respectively. The black solid curves represent the magnetic scattering coefficient in (a) and (d), and the electric scattering coefficient in (b) and (e).

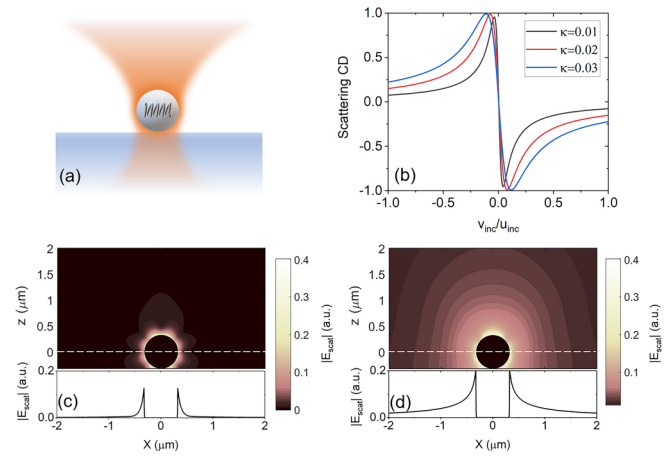

FIG. 4. (a) The light scattering by a chiral sphere on substrate. (b) The scattering CD when the ratio of $v_{\text{inc}}/u_{\text{inc}}$ is varied from -1 to 1, when $\kappa = 0.01,\ 0.02$, and 0.03. (c) The scattering field $|\mathbf{E}_{\text{scat}}|$ under $\mathbf{E}^{(-)}$. (d) The scattering field $|\mathbf{E}_{\text{scat}}|$ under $\mathbf{E}^{(+)}$. The light frequency is $f = 294.463$ THz in (b)–(d). The ratio of $v_{\text{inc}}/u_{\text{inc}}$ is $-1/26$ in (c) and (d). $|\mathbf{E}_{\text{scat}}|$ along the horizontal dash lines are shown in the lower panels of (c) and (d).

lead to the completely destructive interference, resulting in the excitation of anapole states [26–32]. With the illumination of $\mathbf{E}^{(+)}$, the amplitude of the MD is almost unchanged as shown in Fig. 3(d). However, the anapole state is broken because the components of the scattering field contributed by ED and TD cannot be canceled, as shown in Figs. 3(e) and 3(f), respectively. By switching the incident field from $\mathbf{E}^{(-)}$ to $\mathbf{E}^{(+)}$, the condition of complete nonradiating state is no longer fulfilled. Therefore, it is the chirality-sensitive anapole state that enables the measurement of maximum scattering CD.

Next, we will use Eqs. (43) and (44) to further elaborate the mechanism of the chirality-sensitive anapole state. Because the parameters of $\gamma_n^{(a)}$ and $\gamma_n^{(b)}$ are related to the perturbation terms, their values are usually much smaller than $\Gamma_n^{(a)}$ and $\Gamma_n^{(b)}$, resulting in small G_n in Eq. (43). However, it can be found that the maximum scattering CD analyzed in Fig. 3 requires the condition of $\Gamma_1^{(a)} = 0$, whose physical meaning can be further clarified below: according to Eq. (32), $\Gamma_1^{(a)} = 0$ directly leads to $A_1 = 0$. As the nonchiral part of a_1, A_1 is mainly contributed by the zeroth-order scattering process in Fig. 1(a). In other words, the excitation of MD in the reference structure (i.e., the nonchiral sphere) is completely suppressed at $f = 294.46$ THz under the designed incident field. Considering that $\Gamma_1^{(a)} = 0$, the condition of Eq. (44) can be simpified as $v_{\text{inc}}/u_{\text{inc}} = \gamma_1^{(b)}/\Gamma_1^{(b)}$, indicating that the chiral part and nonchiral part of the electric scattering coefficient in Eqs. (34) and (35) are equal (i.e., $B_1 = B'_1$). The electric scattering coefficient b_1 also becomes zero when the sphere is illuminated by $\mathbf{E}^{(-)}$ (i.e., $b_1 = B_1 - B'_1$). Therefore, the nonradiating state is due to the destructive interference not only between the scattering field components radiated by ED and TD, but also between the chiral and nonchiral parts of the scattering field. In contrast, if the incident field is switched to $\mathbf{E}^{(+)}$, the electric scattering coefficient becomes nonzero (i.e., $b_1 = B_1 + B'_1$). In this situation, the scattering fields radiated by the ED and TD cannot be canceled mutually in the far field under the illumination of $\mathbf{E}^{(+)}$. As a result, the condition of the anapole state is not fulfilled as shown in Figs. 3(e) and 3(f).

For the other peak condition at $f = 241.46$ THz with $u_{\text{inc}}/v_{\text{inc}} = 1/55$, the mechanism of maximum scattering CD can also be explained by the excitation of anapole states using the multipole expansion method (see Appendix D). It should be noted that the actual conditions for these two peaks at $u_{\text{inc}}/v_{\text{inc}} = -26$ and $1/55$ are different; i.e., when the chirality of the incident field is inversed, the anapole state can be maintained for the peak at $u_{\text{inc}}/v_{\text{inc}} = 1/55$ but not for $u_{\text{inc}}/v_{\text{inc}} = -26$. Nevertheless, this subtle difference in physics does not change the key mechanism of the maximum scattering CD, i.e., the excitation of anapole states. Next, we employ numerical simulation to demonstrate the feasibility to realize the maximized CD response of the Mie chiral sphere on substrate. The influence of the chiral parameter on the excitation condition of maximized CD will also be analyzed.

V. NUMERICAL SIMULATION RESULTS

In this section, the numerical simulation based on T-matrix method is used to verify the maximized scattering CD of the Mie chiral sphere on substrate in Fig. 4(a) [33,34]. The parameters of the sphere (i.e., R_s, ε_s, μ_s, and κ) remain the same as in Sec. III. The refractive index of the substrate is

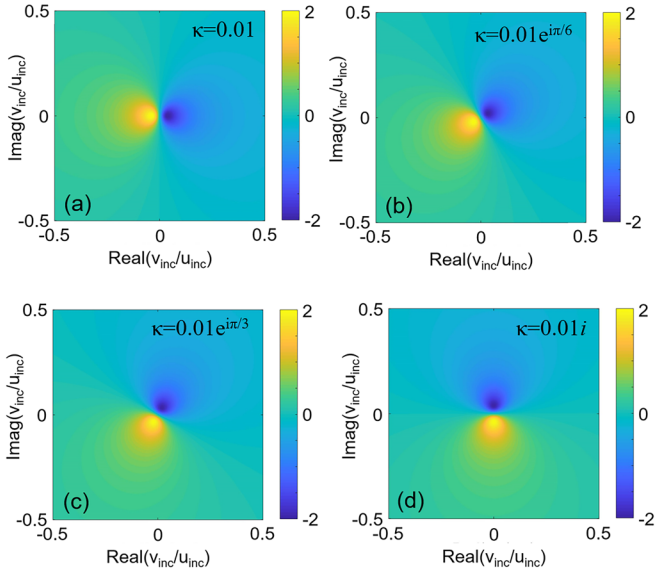

FIG. 5. The scattering CD (i.e., g factor) in the complex plane of $v_{\rm inc}/u_{\rm inc}$. The values of the chiral parameters are 0.01, $0.01e^{i\pi/6}$, $0.01e^{i\pi/3}$, and $0.01i$ in (a)–(d), respectively.

1.37. In Fig. 4(b), the scattering CD is calculated when the ratio of $v_{\rm inc}/u_{\rm inc}$ is varied from -1 to 1. The frequency of the incident light is selected at 294.46 THz, which has been determined in Fig. 1(c). The chiral parameter is chosen as 0.01, 0.02, and 0.03. For $\kappa = 0.01$, the maximum CD can be obtained at $v_{\rm inc}/u_{\rm inc} = -1/26$, which can be well predicted by Eq. (44). Although the ratio of $v_{\rm inc}/u_{\rm inc}$ for maximum CD depends on the chiral parameter, one can also find the optimized excitation condition for different κ values by tuning the ratio of $v_{\rm inc}/u_{\rm inc}$. To clearly demonstrate this maximum chiral response, the pure scattering field excited by $\mathbf{E}^{(-)}$ and $\mathbf{E}^{(+)}$ with $v_{\rm inc}/u_{\rm inc} = -1/26$ are shown in Figs. 4(c) and 4(d), respectively. Furthermore, the amplitude of $|\mathbf{E}_{\rm scat}|$ along the horizontal dashed lines are plotted in the lower panels. One can see that the scattering field is strongly confined in the near field in Fig. 4(c), but can propagate to the far field under the illumination of an incident field with the mirror chirality [Fig. 4(d)]. As a result, the scattering power is zero and nonzero under $\mathbf{E}^{(-)}$ and $\mathbf{E}^{(+)}$ respectively, leading to the maximized value for the scattering CD.

The strategy to achieve the maximum CD is also applicable when the chiral parameter is a complex number. For the sphere with weak chirality, the frequency for the chirality-sensitive anapole state is determined by the reference structure (i.e., the nanosphere with $\kappa = 0$). The value of κ is related to the specific incident field to excite the desired state. Therefore, one can adjust the ratio of $v_{\rm inc}/u_{\rm inc}$ to achieve the maximum scattering CD. To analyze the influence of imaginary part of the chiral parameter κ_s, the chiral parameters of 0.01, $0.01\exp(i\pi/6)$, $0.01\exp(i\pi/3)$, and $0.01i$ are used in the calculation. The light frequency is $f_0 = 294.46\,\text{THz}$. In Fig. 5, the values of scattering CD are calculated under different ratios of $v_{\rm inc}/u_{\rm inc}$, respectively. It can be seen that when κ is a complex number, the optimized value $v_{\rm inc}/u_{\rm inc}$ should be searched in the complex plane around the original point to achieve the maximum scattering CD.

VI. CONCLUSIONS

This work proposed a strategy to design the optical field to realize the maximum scattering CD (i.e., $g = 2$) for a chiral Mie nanosphere. Using multipole analysis, we reveal that the maximum CD effect originates from the excitation of anapole states. This remarkable maximized scattering CD has not been reported before since the required special condition of the incident field was unknown. The maximum chiral response of chiral spheres has been numerically simulated. Currently, chiral light-matter interaction is enhanced by seeking the optical field with strong optical chirality at a local point (e.g., [14,16–20]). However, this route is only viable for a Rayleigh chiral scatterer. The model in this work provides a guideline to globally design the incident field to realize the maximum CD response from Mie spheres. Although the electromagnetic chirality of the Mie sphere is weak (i.e., the κ value is small), the maximum CD response (i.e., g factor) can still be achieved by manipulating the incident field. The extended boundary condition method can be employed to calculate T matrix for homogeneous nonspherical particles, which may be explored to further extend the model to more general cases.

ACKNOWLEDGMENTS

Our work was supported by the National Natural Science Foundation of China (Projects No. 62075132 and No. 92050202) and by the Natural Science Foundation of Shanghai (Grant No. 22ZR1443100). Q.G.'s baseline was supported by PSE of KAUST.

APPENDIX A: EXPRESSIONS OF T_n AND S_n

In Eqs. (9)–(12), the expression of T_n^a, T_n^b, T_n^c, and T_n^d can be expressed as Eqs. (A1)–(A4) [23]:

$$T_n^a = \frac{Z_0\psi_n(k_0R_s)\psi'_n(k_1R_s) - Z_1\psi_n(k_1R_s)\psi'_n(k_0R_s)}{Z_1\psi_n(k_1R_s)\xi'_n(k_0R_s) - Z_0\xi_n(k_0R_s)\psi'_n(k_1R_s)}, \quad \text{(A1)}$$

$$T_n^b = \frac{Z_0\psi_n(k_1R_s)\psi'_n(k_0R_s) - Z_1\psi_n(k_0R_s)\psi'_n(k_1R_s)}{Z_1\xi_n(k_0R_s)\psi'_n(k_1R_s) - Z_0\psi_n(k_1R_s)\xi'_n(k_0R_s)}, \quad \text{(A2)}$$

$$T_n^c = \frac{Z_1k_1\psi_n(k_0R_s)\xi'_n(k_0R_s) - Z_1k_1\xi_n(k_0R_s)\psi'_n(k_0R_s)}{Z_1k_0\psi_n(k_1R_s)\xi'_n(k_0R_s) - Z_0k_0\xi_n(k_0R_s)\psi'_n(k_1R_s)}, \quad \text{(A3)}$$

$$T_n^d = \frac{Z_1k_1\xi_n(k_0R_s)\psi'_n(k_0R_s) - Z_1k_1\psi_n(k_0R_s)\xi'_n(k_0R_s)}{Z_1k_0\xi_n(k_0R_s)\psi'_n(k_1R_s) - Z_0k_0\psi_n(k_1R_s)\xi'_n(k_0R_s)}, \quad \text{(A4)}$$

where R_s is the radius of the sphere. $\psi_n(\alpha)$ and $\xi_n(\alpha)$ are the Riccati-Bessel functions.

In Eqs. (26)–(29), the expressions of S_n^a, S_n^b, S_n^c, and S_n^d can be expressed as Eqs. (A5)–(A8)

$$S_n^a = \frac{Z_0k_0\xi_n^{(1)}(k_1R_s)\psi'_n(k_1R_s) - Z_0k_0\psi_n(k_1R_s)\xi'_n(k_1R_s)}{Z_0k_1\xi_n^{(1)}(k_0R_s)\psi'_n(k_1R_s) - Z_1k_1\psi_n(k_1R_s)\xi'_n(k_0R_s)}, \quad \text{(A5)}$$

$$S_n^b = \frac{Z_0k_0\psi_n(k_1R_s)\xi'_n(k_1R_s) - Z_0k_0\xi_n(k_1R_s)\psi'_n(k_1R_s)}{Z_0k_1\psi_n(k_1R_s)\xi'_n(k_0R_s) - Z_1k_1\xi_n(k_0R_s)\psi'_n(k_1R_s)}, \quad \text{(A6)}$$

$$S_n^c = \frac{Z_1\xi_n^{(1)}(k_1R_s)\xi'_n(k_0R_s) - Z_0\xi_n(k_0R_s)\xi'_n(k_1R_s)}{Z_0\xi_n(k_0R_s)\psi'_n(k_1R_s) - Z_1\psi_n(k_1R_s)\xi'_n(k_0R_s)}, \quad \text{(A7)}$$

$$S_n^d = \frac{Z_1\xi_n(k_0R_s)\xi'_n(k_1R_s) - Z_0\xi_n^{(1)}(k_1R_s)\xi'_n(k_0R_s)}{Z_0\psi_n(k_1R_s)\xi'_n(k_0R_s) - Z_1\xi_n(k_0R_s)\psi'_n(k_1R_s)}. \quad \text{(A8)}$$

APPENDIX B: MIRROR OPERATION ON VSH

The vector spherical harmonics (VSHs) are expressed as [23]

$$Rg\mathbf{M}_{mn} = \gamma_{mn} j_n(r)\left[im\pi_n^m(\theta)\hat{\theta} - \tau_n^m(\theta)\hat{\phi}\right]e^{im\phi}, \quad \text{(B1)}$$

$$Rg\mathbf{N}_{mn} = \gamma_{mn} n(n+1)\frac{j_n(kr)}{kr}P_n^m(\cos\theta)e^{im\phi}\hat{r} + \gamma_{mn}\frac{\psi'_n(kr)}{kr}\left[\tau_n^m(\theta)\hat{\theta} + im\pi_n^m(\theta)\hat{\phi}\right]e^{im\phi}, \quad \text{(B2)}$$

$$\mathbf{M}_{mn} = \gamma_{mn} h_n^{(1)}(r)\left[im\pi_n^m(\theta)\hat{\theta} - \tau_n^m(\theta)\hat{\phi}\right]e^{im\phi}, \quad \text{(B3)}$$

$$\mathbf{N}_{mn} = \gamma_{mn} n(n+1)\frac{h_n^{(1)}(kr)}{kr}P_n^m(\cos\theta)e^{im\phi}\hat{r} + \gamma_{mn}\frac{\xi'_n(kr)}{kr}\left[\tau_n^m(\theta)\hat{\theta} + im\pi_n^m(\theta)\hat{\phi}\right]e^{im\phi}. \quad \text{(B4)}$$

In Eqs. (B1)–(B4), γ_{mn} is a prefactor for the multipole order of $(m,\ n)$,

$$\gamma_{mn} = \sqrt{\frac{(2n+1)(n-m)!}{4\pi n(n+1)(n+m)!}}. \quad \text{(B5)}$$

Here, j_n and $h_n^{(1)}$ are the spherical Bessel and the first kind spherical Hankel functions. P_n^m is the associated Legendre function. The functions of π_n^m and τ_n^m are defined as

$$\pi_n^m(\theta) = \frac{P_n^m(\cos\theta)}{\sin\theta}, \quad \text{(B6)}$$

$$\tau_n^m(\theta) = \frac{dP_n^m(\cos\theta)}{d\theta}. \quad \text{(B7)}$$

For mirror operation in spherical coordinate, the following transformations are performed simultaneously, i.e., $r \Rightarrow r$, $\theta \Rightarrow \theta$, $\phi \Rightarrow \pi - \phi$, $\hat{r} \Rightarrow \hat{r}$, $\hat{\theta} \Rightarrow \hat{\theta}$, and $\hat{\phi} \Rightarrow -\hat{\phi}$. Therefore, $\hat{\mathbf{M}}Rg\mathbf{M}_{mn} = \gamma_{mn} j_n(\rho)[im\pi_n^m(\theta)\hat{\theta} + \tau_n^m(\theta)\hat{\phi}]e^{-im\phi}$, where $\hat{\mathbf{M}}$ is the mirror operator. The relation between the associated Legendre functions with (m, n) and $(-m, n)$ can be expressed as

$$P_n^{-m}(\cos\theta) = (-1)^m\frac{(n-m)!}{(n+m)!}P_n^m(\cos\theta). \quad \text{(B8)}$$

By using the relations in Eqs. (B1)–(B8), it can be proved that

$$\hat{\mathbf{M}}Rg\mathbf{M}_{mn} = (-1)^{m+1}Rg\mathbf{M}_{-m,n}, \quad \text{(B9)}$$

$$\hat{\mathbf{M}}Rg\mathbf{N}_{mn} = (-1)^m Rg\mathbf{N}_{-mn}, \quad \text{(B10)}$$

$$\hat{\mathbf{M}}\mathbf{M}_{mn} = (-1)^{m+1}\mathbf{M}_{-m,n}, \quad \text{(B11)}$$

$$\hat{\mathbf{M}}\mathbf{N}_{mn} = (-1)^m\mathbf{N}_{-mn}. \quad \text{(B12)}$$

Equations (B9) and (B10) can be employed to obtain the incident field with the inversed chirality. Therefore, for the incident field of $\mathbf{E}^{(+)} = u_{\text{inc}}Rg\mathbf{M}_{1,1} + v_{\text{inc}}Rg\mathbf{N}_{1,1}$, its mirror field should be $\mathbf{E}^{(-)} = u_{\text{inc}}Rg\mathbf{M}_{-1,1} - v_{\text{inc}}Rg\mathbf{N}_{-1,1}$.

APPENDIX C: SCATTERING CD OF NANOSPHERE UNDER CPL

To verify the multiscattering model in this work, the rigorous calculation based on Lorenz-Mie theory is carried out under the illumination of CPL. The T matrix for the chiral sphere in free space (with the refractive index of n_0) can be expressed as [34,35]

$$\mathbf{T} = \begin{bmatrix} T_{11}^{(1)} & T_{12}^{(1)} \\ T_{21}^{(1)} & T_{22}^{(1)} \end{bmatrix}^{-1}\begin{bmatrix} T_{11}^{(2)} & T_{12}^{(2)} \\ T_{21}^{(2)} & T_{22}^{(2)} \end{bmatrix}. \quad \text{(C1)}$$

The elements in Eq. (C1) are given below:

$$T_{11}^{(1)} = iZ_0\varepsilon_1\xi_n(k_0R_s)\psi'_n(k_RR_s) - i\sqrt{\varepsilon_1\mu_1}\psi_n(k_RR_s)\xi'_n(k_0R_s), \quad \text{(C2)}$$

$$T_{12}^{(1)} = iZ_0\varepsilon_1\psi_n(k_RR_s)\xi'_n(k_0R_s) - i\sqrt{\varepsilon_1\mu_1}\xi_n(k_0R_s)\psi'_n(k_RR_s), \quad \text{(C3)}$$

$$T_{21}^{(1)} = -Z_0\sqrt{\varepsilon_1\mu_1}\xi_n(k_0R_s)\psi'_n(k_LR_s) + \mu_1\psi_n(k_LR_s)\xi'_n(k_0R_s), \quad \text{(C4)}$$

$$T_{22}^{(1)} = Z_0\sqrt{\varepsilon_1\mu_1}\psi_n(k_LR_s)\xi'_n(k_0R_s) - \mu_1\xi_n(k_0R_s)\psi'_n(k_LR_s), \quad \text{(C5)}$$

$$T_{11}^{(2)} = -iZ_0\varepsilon_1\psi_n(k_0R_s)\psi'_n(k_RR_s) + i\sqrt{\varepsilon_1\mu_1}\psi_n(k_RR_s)\psi'_n(k_0R_s), \quad \text{(C6)}$$

$$T_{12}^{(2)} = -iZ_0\varepsilon_1\psi_n(k_RR_s)\psi'_n(k_0R_s) + i\sqrt{\varepsilon_1\mu_1}\psi_n(k_0R_s)\psi'_n(k_RR_s), \quad \text{(C7)}$$

$$T_{21}^{(2)} = Z_0\sqrt{\varepsilon_1\mu_1}\psi_n(k_0R_s)\psi'_n(k_LR_s) - \mu_1\psi_n(k_LR_s)\psi'_n(k_0R_s), \quad \text{(C8)}$$

$$T_{22}^{(2)} = -Z_0\sqrt{\varepsilon_1\mu_1}\psi_n(k_LR_s)\psi'_n(k_0R_s) + \mu_1\psi_n(k_0R_s)\psi'_n(k_LR_s). \quad \text{(C9)}$$

The two wave vectors inside the sphere are $k_{L/R} = \omega\sqrt{\varepsilon_s\mu_s} \mp \omega\kappa_s$. The radius of the sphere is R_s. The scattering coefficients can be calculated by $[\mathbf{a}\ \mathbf{b}]^T = \mathbf{T}[\mathbf{u}\ \mathbf{v}]^T$. Then the scattering power can be calculated by the scattering coefficients of a_{mn} and b_{mn}.

In our model, the radius of the sphere is $R_s = 320$ nm. For $\varepsilon_s = 9$, $\mu_s = 1$, and $\kappa_s = 0.01$, the scattering CD under the incidence of CPL is calculated as shown in Fig. 6. Within the optical frequency range 176.5–333.3 THz, the value of the scattering CD is in the range $[-0.114, 0.054]$. The analytical method can be used to verify the multiscattering model in this work. For comparison, the scattering CD spectrum calculated by the multiscattering model is shown by the red dots in

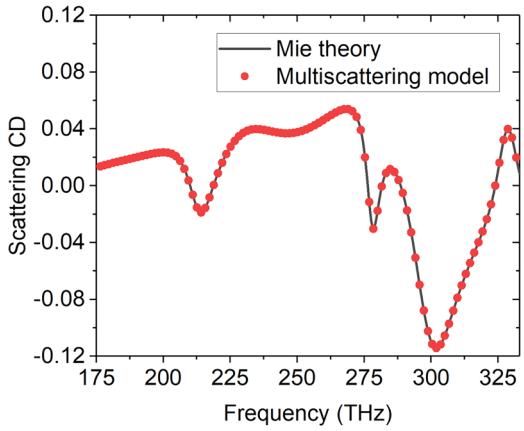

FIG. 6. The scattering CD spectrum for chiral sphere under the illumination of CPL. The black curve and the red dots represent the results calculated by the Mie theory and multiscattering model, respectively.

Fig. 6, which proves that the multiscattering model is accurate to describe the chiral response of the Mie sphere with weak chirality.

APPENDIX D: MAXIMUM CD AT 241.46 THz

To explain the mechanism of maximum scattering CD at $f = 241.46\,\mathrm{THz}$, intensities of the three moments for the sphere and the electric and magnetic scattering coefficients (i.e., a_1 and b_1) are calculated in Fig. 7. The incident field is $\mathbf{E}^{(\pm)} = u_{\mathrm{inc}} Rg\mathbf{M}_{\pm1,1} \pm v_{\mathrm{inc}} Rg\mathbf{N}_{\pm1,1}$ with $u_{\mathrm{inc}}/v_{\mathrm{inc}} = 1/55$. Figures 7(a)–7(c) show the calculation results when the chiral sphere is illuminated by $\mathbf{E}^{(-)}$. At the frequency of 241.46 THz, both scattering coefficients a_1 in Fig. 7(a) and b_1 in Fig. 7(b) are zero, indicating that the sphere is at the completely nonradiating state. Specifically, a_1 can be well predicted by the amplitude of MD in Fig. 7(a), while b_1 is mainly contributed by ED and TD [see the amplitudes of b_1, ED, and TD in Fig. 7(b)]. At $f = 241.46\,\mathrm{THz}$, the amplitudes of ED and TD are equal, but their phases are opposite [see the vertical dashed line through Figs. 7(a)–7(c)], which indicates the excitation of anapole state in the sphere. With the illumination of $\mathbf{E}^{(+)}$, the amplitudes of ED and TD are almost unchanged as shown in Figs. 7(e) and 7(f). It means the anapole state is stable during the inversion of optical chirality, which is different from the case in Fig. 3. However, by switching the incident field from $\mathbf{E}^{(-)}$ to $\mathbf{E}^{(+)}$, the dip of MD amplitude at $f = 241.46\,\mathrm{THz}$ disappears as shown in Fig. 7(d). Therefore, the maximum CD condition can also be enabled due to the excitation of anapole states.

To further understand the mechanism of the dependence of the magnetic scattering coefficient a_1 to the chirality of the incident field, Eqs. (32) and (33) should be considered.

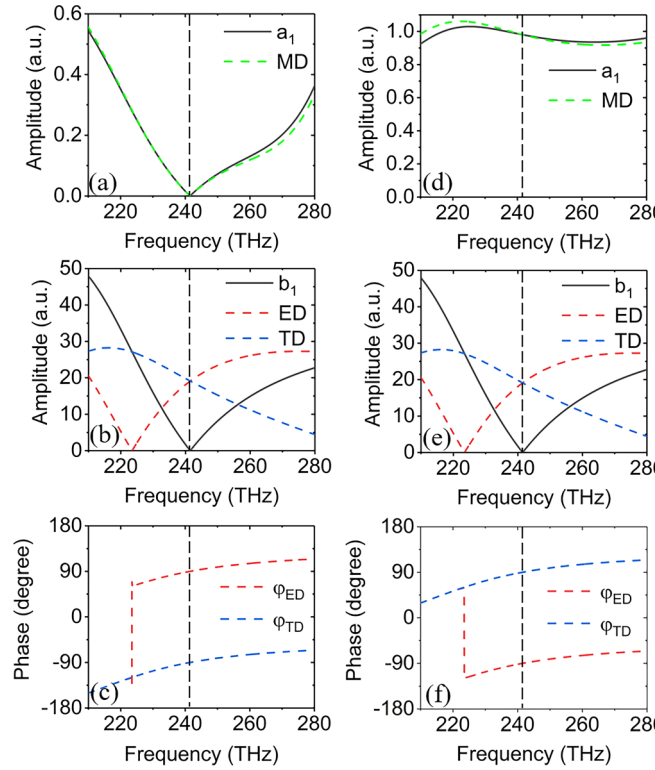

FIG. 7. The spectra of scattering coefficients and the complex amplitudes of three types dipoles for the incident field with $u_{\mathrm{inc}}/v_{\mathrm{inc}} = 1/55$. The results in (a)–(c) are under the incidence of $\mathbf{E}^{(-)}$, and in (d)–(f) for $\mathbf{E}^{(+)}$.

The maximum scattering CD analyzed in Fig. 7 requires the condition of $\Gamma_n^{(b)} = 0$, whose physical meaning can be further clearified below: It directly leads to $B_{mn} = 0$ according to Eq. (34). As the nonchiral part of b_{mn}, B_{mn} is mainly contributed by the zeroth-order scattering process in Fig. 1(a). It means that the anapole state in the reference structure (i.e., nonchiral sphere) and the component of $Rg\mathbf{N}_{mn}$ in the incident field cannot be scattered. The condition to obtain the maximum CD in Eq. (44) can be simplified as $u_{mn}/v_{mn} = \gamma_n^{(a)}/\Gamma_n^{(a)}$, whose value is much smaller than 1. Therefore, $Rg\mathbf{N}_{mn}$ is the dominant component of the incident field. The anapole state excited by $\mathbf{E}^{(-)}$ can be maintained when inversing the chirality of the incident field. The condition of $u_{mn}/v_{mn} = \gamma_n^{(a)}/\Gamma_n^{(a)}$ means that the chiral part and the nonchiral part of the magnetic scattering coefficient in Eqs. (32) and (33) are equal (i.e., $A_{mn} = A'_{mn}$). The magnetic scattering coefficient a_{mn} also becomes zero when the sphere is illuminated by $\mathbf{E}^{(-)}$ (i.e., $a_{mn} = A_{mn} - A'_{mn}$). If the incidence is switched to $\mathbf{E}^{(+)}$, the magnetic scattering coefficient becomes nonzero (i.e., $a_{mn} = A_{mn} + A'_{mn}$). This is the key reason resulting in the disappearance of the dip of a_1 as shown in Fig. 7(d).

[1] L. D. Barron, *Molecular Light Scattering and Optical Activity* (Cambridge University Press, Cambridge, England, 2004).

[2] A. B. Harris, R. D. Kamien, and T. C. Lubensky, Molecular chirality and chiral parameters, Rev. Mod. Phys. **71**, 1745 (1999).

[3] Y. Inoue and V. Ramamurthy, *Chiral Photochemistry* (Marcel Dekker, New York, 2004).

[4] J. Mun, M. Kim, Y. Yang, T. Badloe, J. Ni, Y. Chen, C. W. Qiu, and J. Rho, Electromagnetic chirality: from fundamentals

to nontraditional chiroptical phenomena, Light Sci. Appl. **9**, 139 (2020).

[5] M. Hentschel, M. Schäferling, X. Duan, H. Giessen, and N. Liu, Chiral plasmonics, Sci. Adv. **3**, e1602735 (2017).

[6] L. V. Poulikakos, P. Gutsche, K. M. McPeak, S. Burger, J. Niegemann, C. Hafner, and D. J. Norris, Optical chirality flux as a useful far-field probe of chiral near fields, ACS Photonics **3**, 1619 (2016).

[7] C. Kramer, M. Schäferling, T. Weiss, H. Giessen, and T. Brixner, Analytic optimization of near-field optical chirality enhancement, ACS Photonics **4**, 396 (2017).

[8] S. Both, M. Schäferling, F. Sterl, E. A. Muljarov, H. Giessen, and T. Weiss, Nanophotonic chiral Sensing: how does it actually Work?, ACS Nano **16**, 2822 (2022).

[9] J. K. Gansel, M. Thiel, M. S. Rill, M. Decker, K. Bade, V. Saile, G. von Freymann, S. Linden, and M. Wegener, Gold helix photonic metamaterial as broadband circular polarizer, Science **325**, 1513 (2009).

[10] J. Sun, H. Hu, D. Pan, S. Zhang, and H. Xu, Selectively depopulating valley-polarized excitons in monolayer MoS_2 by local chirality in single plasmonic nanocavity, Nano Lett. **20**, 4953 (2020).

[11] Y. Cui, L. Kang, S. Fan, S. Rodrigues, and W. Cai, Giant chiral optical response from a twisted-arc metamaterial, Nano Lett. **14**, 1021 (2014).

[12] I. Fernandez-Corbaton, M. Fruhnert, and C. Rockstuhl, Objects of Maximum Electromagnetic Chirality, Phys. Rev. X **6**, 031013 (2016).

[13] M. V. Gorkunov, A. A. Antonov, and Y. S. Kivshar, Metasurfaces with Maximum Chirality Empowered by Bound States in the Continuum, Phys. Rev. Lett. **125**, 093903 (2020).

[14] Y. Tang and A. E. Cohen, Optical Chirality and Its Interaction with Matter, Phys. Rev. Lett. **104**, 163901 (2010).

[15] D. Lipkin, Existence of a new conservation law in electromagnetic theory, J. Math. Phys. (N.Y.) **5**, 696 (1964).

[16] Y. Tang and A. E. Cohen, Enhanced enantioselectivity in excitation of chiral molecules by superchiral light, Science **332**, 333 (2011).

[17] K. C. van Kruining, R. P. Cameron, and J. B. Götte, Superpositions of up to six plane waves without electric-field interference, Optica **5**, 1091 (2018).

[18] H. Hu, Q. Gan, and Q. Zhan, Generation of a Nondiffracting Superchiral Optical Needle for Circular Dichroism Imaging of Sparse Subdiffraction Objects, Phys. Rev. Lett. **122**, 223901 (2019).

[19] K. Du, P. Li, H. Wang, K. Gao, R. B. Liu, F. Lu, W. Zhang, and T. Mei, Optical chirality enhancement in hollow silicon disk by dipolar interference, Adv. Opt. Mater. **9**, 2001771 (2021).

[20] C. He, G. Yang, Y. Kuai, S. Shan, L. Yang, J. Hu, D. Zhang, Q. Zhang, and G. Zou, Dissymmetry enhancement in enantioselective synthesis of helical polydiacetylene by application of superchiral light, Nat. Commun. **9**. 5117 (2018).

[21] Y. Q. Yang and S. I. Bozhevolnyi, Nonradiating anapole states in nanophotonics: from fundamentals to applications, Nanotechnology **30**, 204001 (2019).

[22] J. Ni, S. Liu, D. Wu, Z. Lao, Z. Wang, K. Huang, S. Ji, J. Li, Z. Huang, Q. Xiong, Y. Hu, J. Chu, and C. W. Qiu, Gigantic vortical differential scattering as a monochromatic probe for multiscale chiral structures, Proc. Natl Acad. Sci. USA **118**, e2020055118 (2021).

[23] M. I. Mishchenko, L. D. Travis, and A. A. Lacis, *Scattering, Absorption and Emission of Light by Small Particles* (Cambridge University Press, Cambridge, England, 2002).

[24] I. V. Lindell, A. H. Sihvola, S. A. Tretyakov, and A. J. Viitanen, *Electromagnetic Waves in Chiral and Bi-Isotropic Media* (Artech House, Norwood, MA, 1994).

[25] J. D. Jackson, *Classical Electrodynamics*, 3rd ed. (John Wiley and Sons, Inc., New York, 1998).

[26] A. E. Miroshnichenko, A. B. Evlyukhin, Y. F. Yu, R. M. Bakker, A. Chipouline, A. I. Kuznetsov, B. Luk'yanchuk, B. N. Chichkov, and Y. S. Kivshar, Nonradiating anapole modes in dielectric nanoparticles, Nat. Commun. **6**, 8069 (2015).

[27] L. Wei, Z. Xi, N. Bhattacharya, and H. P. Urbach, Excitation of the radiationless anapole mode, Optica **3**, 799 (2016).

[28] A. Krasnok, D. Baranov, H. N. Li, M. A. Miri, F. Monticone, and A. Alu, Anomalies in light scattering, Adv. Opt. Photonics **11**, 892 (2019).

[29] J. A. Parker, H. Sugimoto, B. Coe, D. Eggena, M. Fujii, N. F. Scherer, S. K. Gray, and U. Manna, Excitation of Nonradiating Anapoles in Dielectric Nanospheres, Phys. Rev. Lett. **124**, 097402 (2020).

[30] K. V. Baryshnikova, D. A. Smirnova, B. S. Luk'yanchuk, and Y. S. Kivshar, Optical Anapoles: concepts and applications, Adv. Opt. Mater. **7**, 1801350 (2019).

[31] E. Zanganeh, A. Evlyukhin, A. Miroshnichenko, M. Song, E. Nenasheva, and P. Kapitanova, Anapole Meta-Atoms: Nonradiating Electric and Magnetic Sources, Phys. Rev. Lett. **127**, 096804 (2021).

[32] M. I. Tribelsky and A. E. Miroshnichenko, Giant in-particle field concentration and fano resonances at light scattering by high-refractive-index particles, Phys. Rev. A **93**, 053837 (2016).

[33] T. Bauer, S. Orlov, U. Peschel, P. Banzer, and G. Leuchs, Nanointerferometric amplitude and phase reconstruction of tightly focused vector beams, Nat. Photon. **8**, 23 (2014).

[34] H. Hu and Q. Zhan, Enhanced chiral mie scattering by a dielectric sphere within a superchiral light field, Physics **3**, 747 (2021).

[35] C. F. Bohren, Light scattering by an optically active sphere, Chem. Phys. Lett. **29**, 458 (1974).